

Noname manuscript No.  
(will be inserted by the editor)

---

<sup>1</sup> **Monkeypox virus detection using pre-trained deep**  
<sup>2</sup> **learning-based approaches**

<sup>3</sup> **Chiranjibi Sitaula  · Tej Bahadur Shahi**

<sup>4</sup>  
<sup>5</sup> Received: DD Month YEAR / Accepted: DD Month YEAR

<sup>6</sup> **Abstract** Monkeypox virus is emerging slowly with the decline of COVID-  
<sup>7</sup> 19 virus infections around the world. People are afraid of it, thinking that it  
<sup>8</sup> would appear as a pandemic like COVID-19. As such, it is crucial to detect  
<sup>9</sup> them earlier before widespread community transmission. AI-based detection  
<sup>10</sup> could help identify them at the early stage. In this paper, we first compare  
<sup>11</sup> 13 different pre-trained deep learning (DL) models for the Monkeypox virus  
<sup>12</sup> detection. For this, we first fine-tune them with the addition of universal cus-  
<sup>13</sup> tom layers for all of them and analyse using four well-established measures:  
<sup>14</sup> Precision, Recall, F1-score, and Accuracy. After the identification of the best-  
<sup>15</sup> performing DL models, we ensemble them to improve the overall performance  
<sup>16</sup> using a majority voting over the probabilistic outputs obtained from them.  
<sup>17</sup> We perform our experiments on a publicly available dataset, which shows that  
<sup>18</sup> our ensemble method provides Precision, Recall, F1-score, and Accuracy of  
<sup>19</sup> 85.44%, 85.47%, 85.40%, and 87.13%, respectively. These encouraging results  
<sup>20</sup> suggest that the proposed approach is applicable to health practitioners for  
<sup>21</sup> mass screening.

---

C. Sitaula  
Department of Electrical and Computer Systems Engineering, Monash University  
Wellington Rd, VIC 3800  
E-mail: chiranjibi.sitaula@monash.edu

TB. Shahi  
School of Engineering and Technology  
Central Queensland University  
Norman Garden, QLD, 4701, Australia  
and  
Central Department of Computer Science and IT  
Tribhuvan University  
TU Rd, Kirtipur 44618, Kathmandu, Nepal  
E-mail: tejshahi@cdcsit.edu.np

<sup>22</sup> **Keywords** SARS-Cov2 · Classification · Monkeypox · Deep learning ·  
<sup>23</sup> Detection · Pandemic

## 1 Introduction

Monkeypox is an infectious disease caused by the monkeypox virus (MPXV), a member of the orthopoxvirus genus. It was first identified in the monkey in 1959 at a research institute in Denmark, hence it is named as Monkeypox virus [3]. Later, the first case was confirmed in humans in the Republic of Congo in 1970 when a child with smallpox-like symptoms was admitted to the hospital [12]. It transmits to humans through close contact with infected individuals or contaminated objects [14]. Initially, it usually appeared in the African region but recently it has reached over more than 50 countries with 3,413 confirmed cases and one death [28]. Till now, there are two variants of the monkeypox virus known: one, the Central Africa clade and another, the West Africa clade. There is no proper treatment for the monkeypox virus to date. The ultimate solution is the development of a vaccine. The diagnosis of Monkeypox can be performed mainly with the polymerase chain reaction (PCR) method or skin lesion test using electron microscopy. The most trusted method of virus confirmation is PCR, which has also been used for COVID-19 diagnosis in recent years. In addition, artificial intelligence (AI)-based techniques could help detect them with the help of virus image processing and analysis.

With the emerging growth of AI models in various domains such as chest x-ray images [25], fruit image analysis [21], and sentiment analysis [24], the AI models for medical image analysis have been proposed for various virus-related disease detection. For instance, Sandeep et. al.[17] investigated the detection of various skin diseases such as Psoriasis, Chicken Pox, Vitiligo, Melanoma, Ringworm, Acne, Lupus, and Herpes using deep learning (DL)-based methods. They developed a Convolutional Neural Network (CNN) to classify the skin lesion into eight disease classes and compared their solution with the help of the VGG-16 pre-trained model [22]. Their method provided an accuracy of 78% for the detection. Low-cost image analysis for Herpes Zoster Virus (HZV) detection using CNN was proposed in [11]. The early detection of HZV produced an accuracy of 89.6% when tested on 1,000 images. Furthermore, Measles disease detection using a transfer learning approach was implemented by Glock et al. [7]. They achieved a sensitivity of 81.7%, specificity of 97.1%, and accuracy of 95.2% using ResNet-50 model [8] over the diverse rash image dataset. Moreover, a big-data approach for Ebola virus disease detection was proposed in [19] using an ensemble learning approach. They utilized a combination of artificial neural network (ANN) and genetic algorithm (GA) for knowledge extraction over the big data using Apache Spark and Kafka framework. More recently, Ahsan et. al. [1] collected the images of Monkeypox, Chickenpox, Measles and Normal categories using web mining techniques and verified by the experts. Later on, they also evaluated a transfer learning approach with VGG-16 model considering two study techniques [2]. The first

**Table 1** Dataset statistics

Category	Chickenpox	Measles	Monkeypox	Normal	Total
#Number	329	286	587	552	1,754

technique considered the classification of images into two disease classes: Monkeypox and Chickenpox, whereas the second technique augmented the images. They reported accuracy of (97%) while classifying the monkeypox without data augmentation, whereas the accuracy was decreased to 78% with augmentation.

Although the proposed methods have provided encouraging results in this domain, they have the following limitations. First, their models only deal with binary classification and have limited performance. Second, they only consider VGG-16 for transfer learning, which lacks to identify the best-performing pre-trained DL methods and their best combinations. Third, their models have insufficient interpretability, which is crucial for health practitioners to analyse the details.

To address the aforementioned limitations, we first resort to the 13 pre-trained DL models and fine-tune them with the same approach. Second, we evaluate the performance of each DL model using averaged Precision, Recall, F1-score and Accuracy over 5 folds. Third, we ensemble the best-performing models to improve the performance.

The main **contributions** in this paper are as follows:

- Propose to use a common fine-tuned architecture for all 13 pre-trained DL models for MonkeyPox detection and compare them;
- Perform an ablative study to select the best-performing DL models for ensemble learning; and
- Show the explain-ability using Grad-CAM [20] and LIME [15] of best-performing DL model.

## 2 Materials and methods

### 2.1 Dataset

Herein, we use a publicly available monkeypox image dataset [1, 2]. The dataset has different sub-folders, including datasets with and without augmentations. Given that DL models prefer augmented images to learn meaningful information more accurately, we use them in this study. Table 1 shows the number of images from the augmented folder per category.

## 2.2 Evaluation metrics

We use four widely-used performance metrics such as Precision (Eq. (1)), Recall (Eq. (2)), F1-score (Eq. (3)), and Accuracy (Eq. (4)).

$$P = \frac{TP}{TP + FP}, \quad (1)$$

$$R = \frac{TP}{TP + FN}, \quad (2)$$

$$F = 2 \times \frac{P \times R}{P + R}, \quad (3)$$

$$A = \frac{TP + TN}{TP + TN + FP + FN}, \quad (4)$$

where  $TP$ ,  $TN$ ,  $FP$ , and  $FN$  represent true positive, true negative, false positive, and false negative, respectively. Similarly,  $P$ ,  $R$ ,  $F$ , and  $A$  represent Precision, Recall, F1-score, and Accuracy, respectively.

## 2.3 Pre-trained DL models

The availability of various DL models trained on a large dataset, called ImageNet [6], made a significant progress in image classification and computer vision tasks. More precisely, when the availability of expert-labelled data is limited to some domains such as biomedical image analysis, a most common approach is to utilise these pre-trained DL models for transfer learning [13]. This is helpful to boost the performance in a limited data setting because transfer learning allows the DL models trained on large datasets to transfer learned knowledge to a small domain-specific dataset.

We choose 13 pre-trained DL models in this study. These pre-trained model ranges from heavy-weight DL models such as VGG-16 [22], InceptionV3 and Xception [4] to light-weight models such as MobileNet [9], and EfficientNet [27]. The overall pipeline of the training process for those models is shown in Fig. 1. We use the same customisation for all pre-trained models. A brief discussion of each pre-trained DL model is presented in the next subsections.

### 2.3.1 VGG

The Visual geometry group (VGG) at Oxford University developed a Convolutional Neural Network (CNN), popularly known as VGG-16, which won the ImageNet [6] challenge in 2014. It consists of 13 Convolutions, 5 Max pooling and 3 Dense layers. It is named as VGG-16 because it has 16 layers that has the learnable weight parameters [22]. An extended version of VGG-16 model, which consists 16 Convolution layers, 5 Max-pooling layers and 3 Dense layers, is known as VGG-19

### 2.3.2 ResNet

The very deep convolutional neural network such as VGG-16 and VGG-19 produced promising results in a large-scale image classification task. However, it is very hard to train a very deep neural network due to a vanishing gradient problem, i.e., the multiplication of small gradient propagated back to the previous layer start vanishing after a certain depth. The researchers aimed to address the vanishing gradient problem by introducing the concept of skip connection, which allows skipping some layers in the network. The group of layers in the network that use such skip connection are known as residual blocks (Res-Blocks), which are the core of ResNet architecture [8]. Here, we utilise two ResNet architectures: ResNet-50 and ResNet-101. The ResNet-50 consists of 48 Convolution layers, 1 Max-pooling, and 1 Average pooling layer, whereas ResNet-101 includes 99 Convolution layers, 1 Max-pooling and 1 Average pooling layer.

### 2.3.3 Inception-V3

The idea of widening the network instead of deepening is implemented in the Inception network, by a team of researchers at Google [26]. Inception network architecture uses the four parallel convolutions layers with different kernel sizes at a given depth of network to extract the image feature at different scales before passing them into the next layer. Here, we utilize a 48-layer deep Inception-v3 network.

### 2.3.4 IncepResNet

With the development of wider and deeper architecture with residual connections such as Inception [26] and ResNet [8] network, researchers exploited the benefit of combining the Inception architecture with the residual connections, and established a novel model called InceptionResNet. We utilise the InceptionResNetV2 network , which consists of 449 layers including Convolutions layers, Pooling layers, Batch normalization layers and so on.

### 2.3.5 Xception

It is an extreme version of the Inception network developed by Google in 2017 [4]. The main idea implemented in Xception is to make the Convolutions operation more efficient in Inception blocks. This was achieved with modified depth-wise separable convolution, which is performed in two steps: point-wise convolution followed by depth-wise convolution. Here, the point-wise convolution changes the dimension and depth-wise convolution represents the channel-wise spatial convolution.

### 2.3.6 MobileNet

The idea of depth-wise convolution was further exploited in a deep neural network architecture, known as MobileNet [9]. In this work, we utilise one version of MobileNet architecture, called MobileNetV2 [18]. The MobileNetV2 is an extended version of MobileNetV1, which consists of 1 regular Convolutions layer, 13 depth-wise separable convolutions blocks and 1 regular Convolutions layer, followed by an Average pooling layer. Whereas, MobileNetV2 added the Expand layer, Residual connections and Projection layers in addition to depth-wise Convolution layers known as a Bottleneck residual block.

### 2.3.7 DenseNet

In DenseNet architecture [10], the idea of skip connection was extended to multiple steps instead of one step direct connection as in ResNet. And, the block designed to use in between such connections is known as Dense block. The main components of DenseNet are connectivity, and Dense blocks. Each layer in Densenet has a direct connection to its all forward layer, thereby establishing  $(L+1)/2$  connections for  $L$  layer. Each Dense block consists of Convolutions layers with the same feature map size but different kernel sizes. In this work, we utilise the DenseNet-121 network, which consists of 120 Convolutions layers and 4 Average pooling layers.

### 2.3.8 EfficientNet

The expansion of CNN on each dimension into width, depth, and resolution was attempted arbitrarily in various deep neural network architectures such as ResNet, DenseNet, Inception, Xception and so on. However, the systematic approach for scaling up the CNN with a fixed set of scaling coefficients was proposed in EfficientNet architecture [27]. The network architecture of EfficientNet consists of three blocks: stem, body and final blocks. The stem and final blocks are common in all variants of EfficientNet while the body differs from one version to another. The stem block consists of input, re-scaling, normalization, padding, convolution, batch normalization and activation layer. The body consists of five modules, where each module has depth-wise convolution, batch normalization and activation layers. In this study, we use three versions of EfficientNet: EfficientNet-B0, EfficientNet-B1 and EfficientNet-B2. The EfficientNet-Bo has 237 layers in total, whereas EfficientNet-B1 and EfficientNet-B2 have 339 layers, excluding the top layer.

## 2.4 Implementation

We implement our proposed model using Keras [5] implemented in Python [16]. During the implementation, we tune the parameters as follows. We first

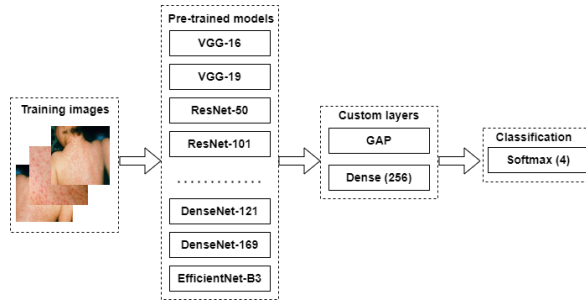


**Fig. 1** High-level workflow to train the pre-trained DL models with custom layers. Note that GAP refers to Global Average Pooling layer and the value inside the small bracket of dense layer represents the number of units under it.

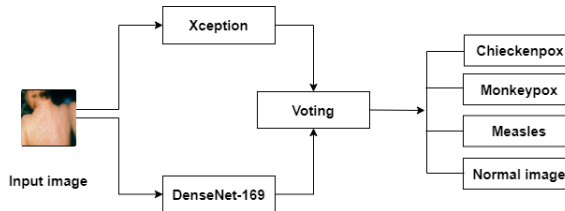


**Fig. 2** Ensemble method between Xception and DenseNet-169 DL models. Note that the Voting block refers to max-voting.

resize each image into 150\*150 as suggested by Sitaula et al. [23]. For augmentation, we apply online data augmentation as follows: rescale=1/255, rotation range=50, width shift range=0.2, height shift range=0.2, shear range=0.25, zoom range=0.1, and channel shift range=20. We set optimizer as 'Adam', batch size as 16, and initial learning rate as 0.0001. To prevent from overfitting, we utilise the learning rate decay over each epoch coupled with the Early stopping criteria.

In our study, we design random five folds (5-cross validation), where each fold contains 70/30 for train/test ratio and report the average performance.

## 2.5 Ensemble approach

To ensemble the multiple DL models, we extract the probabilistic values from each fine-tuned pre-trained model and perform the majority voting approach (refer to Fig. 2). Each of our fine-tuned DL models shows the best-fit to learn the optimal features during the training and testing process (see Fig. 3).

In this study, we choose two best-performing fine-tuned models: Xception and DenseNet-169 based on the empirical study (see Sec. 3.2). Let us assume that the Xception model produces a probabilistic output vector as  $X$  and

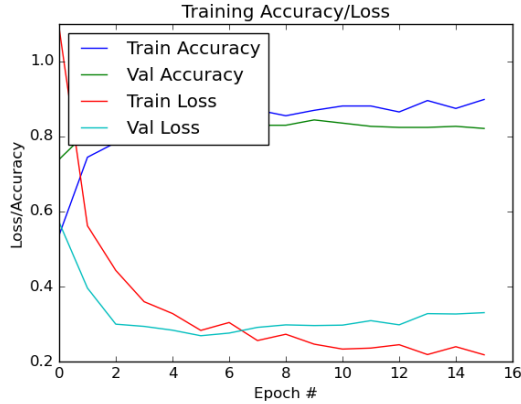


**Fig. 3** Sample train/test plot (fold 1) for accuracy and loss obtained from the fine-tuned Xception DL model.

DenseNet-169 provides a probabilistic output vector as  $D$  with the size equal to the number of classes.

$$X = Xception(I), \quad (5)$$

$$D = DenseNet - 169(I), \quad (6)$$

$$C = \arg \max_c [X, D], \quad (7)$$

where  $I$  is the input image to be classified and  $C$  gives us the index of highest majority value corresponding to the particular class  $c$ .

### 3 Results and discussion

#### 3.1 Comparative study of DL models

We compare the proposed approach with the off-the-shelf pre-trained DL models based on the standard evaluation measures on this dataset. The results are presented in Table 2. Note that the reported results are the averaged performance over 5 different folds (5-fold cross validation).

From Table 2, we notice that the Xception is the second-best performing method among all contenders, whereas it is the best method among 13 pre-trained DL methods (Precision: 85.01%, Recall: 85.14%, F1-score: 85.02%, and Accuracy: 86.51%). We believe that this is because of the Xception's higher ability to extract the discriminating information from the virus images with the help of its point-wise and depth-wise convolution. In addition, our proposed ensemble method is the best-performing method among all contenders

with an accuracy of 87.13%. In terms of other performance metrics such as Precision, Recall and F1-score, we observe that it imparts 85.44% of Precision, 85.47% of Recall and 85.40% of F1-score. This shows that it is 0.43% higher in Precision, 0.33% higher in Recall, and 0.38% higher in F1-score than the second-best performing method (Xception). Furthermore, it imparts 5.26%, 6.3%, and 6.39% higher Precision, Recall, and F1-score, respectively than the least-performing DL method (VGG-16). Such improvement in the result is because of the decision fusion, which helps fuse the decision outcomes from different DL models as the final decision.

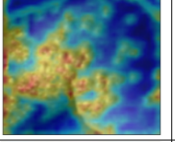
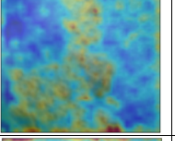
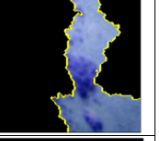
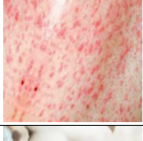
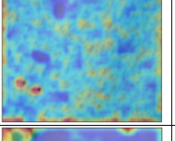
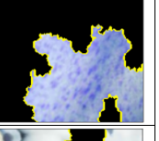
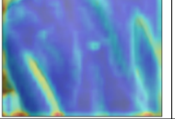
In summary, our proposed common custom layers are appropriate for fine-tuning all 13 pre-trained DL models to achieve optimal accuracy on this dataset. This is shown not only from the best-fit train/test graph but also from the overall performance (from 80.18% to 84.07% for Precision, from 79.17% to 83.74% for Recall, from 70.01% to 83.83% for F1-score and from 82.22% to 86.06% for Accuracy). Similarly, the majority voting approach has also been an interesting option in ensemble learning to exploit the highest decision for the optimal end classification result.

**Table 2** Comparison of pre-trained DL models and ensemble approach using averaged Precision, Recall, F1-score, and Accuracy over 5 different folds.

Methods	P (%)	R (%)	F(%)	A (%)
VGG-16	80.18	79.17	79.01	82.22
VGG-19	81.84	81.90	81.03	82.94
ResNet-50	82.81	82.94	82.82	84.87
ResNet-101	82.69	81.88	82.02	84.98
IncepResNetv2	83.90	83.44	83.62	85.43
MobileNetV2	82.85	81.17	80.98	84.87
InceptionV3	82.51	82.30	82.16	84.53
Xception	85.01	85.14	85.02	86.51
EfficientNet-B0	81.60	81.34	81.40	83.96
EfficientNet-B1	83.69	84.03	83.61	85.09
EfficientNet-B2	82.06	82.67	82.07	83.51
DenseNet-121	83.12	83.00	82.25	84.24
DenseNet-169	84.07	83.74	83.83	86.06
Ensemble approach	<b>85.44</b>	<b>85.47</b>	<b>85.40</b>	<b>87.13</b>

**Table 3** Performance comparison of DL different models combination using Precision, Recall, F1-score and Accuracy. Note that M1=Xception, M2=DenseNet-169, M3=IncepResNetv2, M4=EfficientNet-B1, and M5=ResNet-101.

Model ensemble	P (%)	R (%)	F (%)	A (%)
{M1, M2, M3, M4, M5}	84.03	83.26	83.50	85.83
{M1, M2, M3, M4}	84.63	84.03	84.24	86.23
{M1, M2, M3}	84.55	84.00	84.20	86.17
{M1, M2}	<b>85.44</b>	<b>85.47</b>	<b>85.40</b>	<b>87.13</b>

Label	Image	Grad-CAM	LIME
Monkeypox			
Chickenpox			
Measles			
Normal			

**Fig. 4** Visualisation based on Grad-CAM and LIME for the Xception model.

### 3.2 Candidate model selection for ensemble

We select only those DL models that provide optimal performance in our study. For this, we select the top-5 models and their combinations for decision fusion. The detailed results are presented in Table 3. From Table 3, we observe that the combination of two models (Xception as M1 and DenseNet-169 as M2) provides us with the best performance compared to other combinations.

### 3.3 Explainability

We show the explainability of the DL model using the Gradient-weighted Class Activation Mapping (Grad-CAM) [20] and Local Interpretable Model-Agnostic Explanations (LIME) [15] visualisation techniques. For this, we use the Xception model, which is the best-performing model, on the monkeypox dataset. The outputs are presented in Fig. 4. The Grad-CAM measures the gradient of the output feature map of a selected layer of the network, whereas the LIME is a local model-independent approach to generate the interpretation for a specific case, which transforms the input data into a series of interpretable local representation.

From Fig. 4, we notice that the outputs obtained from the Xception model is able to detect the discriminating regions clearly for the classification. For instance, the Grad-CAM is able to show the virus-infected regions in yellow or dark yellow color and the LIME is able to encircle the potentially infected

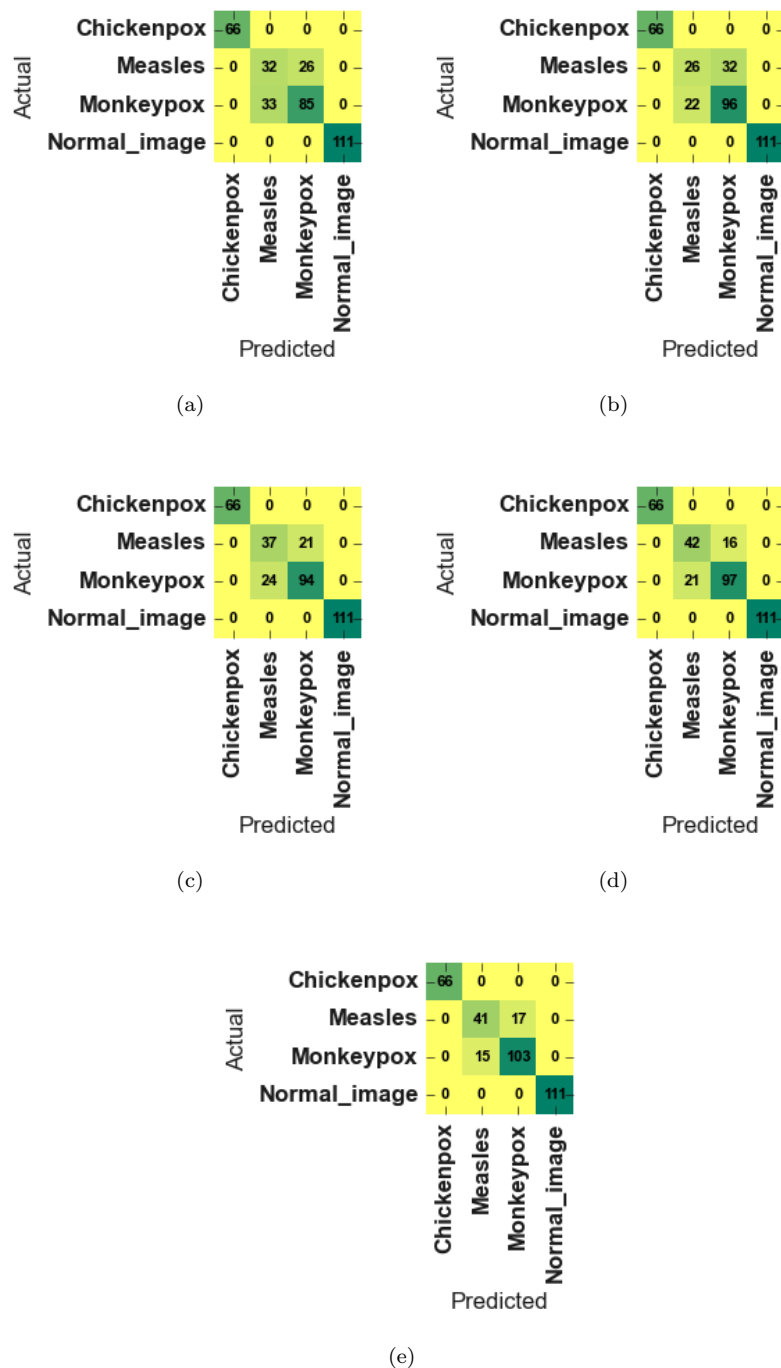


**Fig. 5** Confusion matrix of results obtained for five folds from (a) to (e) from the best performing Xception DL model in our study.

regions with its superpixel on the map. Note that for the Grad-CAM, we set 'block14\_sepconv2\_act' layer from the Xception DL model. And, for the LIME, we set the number of features as 5, the number of samples as 1000, and top labels as 4 for the Xception DL model.

### 3.4 Class-wise study

We study the class-wise performance of the ensemble approach using the confusion matrix, which is shown in Fig. 5. From Fig. 5, different confusion matrices for all five-folds show that our ensemble approach is able to discriminate the images clearly into four different classes. More specifically, our method is able to highly discriminate chickenpox and normal images compared to measles and monkeypox virus. Furthermore, all instances of chickenpox (66) and normal images (111) in the test set are recognised correctly by the proposed model, whereas it is still not perfect to discriminate measles and monkeypox viruses in fold 1 (a). This might be due to the similar features identified by the backbone CNN for two classes: measles and Monkeypox viruses as seen in Grad-CAM visualization 4.

## 4 Conclusion and future works

In this paper, we compared 13 different pre-trained DL models with the help of transfer-learning on the monkeypox dataset. By the help of such comparison using well-established evaluation measures, we identified the best-performing DL models to ensemble them for the overall performance improvement. The evaluation result shows that ensemble approach provides the highest performance (Precision: 85.44%; Recall: 85.47%; F1-score: 85.40%; and Accuracy: 87.13%) during the detection of Monkeypox virus. Also, the Xception DL model provides the second-best performance (Precision: 85.01%; Recall: 85.14%; F1-score: 85.02%; and Accuracy: 86.51%).

There are two major limitations of our work. First, the dataset size is comparatively smaller, so addition of more data could improve the performance further. Second, our AI approach is based on pre-trained DL models, which could be a problem if we would like to deploy them in a memory-constrained setting. So, the design of novel lightweight DL models could be an interesting work to let it work on a limited resource.

## 5 Declarations

### 5.1 Ethical Approval and Consent to participate

Authors declares that no ethical approval is required as the data used in this work are publicly available.

## 5.2 Human and Animal Ethics

Not applicable.

## 5.3 Consent for publication

Not applicable.

## 5.4 Availability of supporting data

All data are publicly available.

## 5.5 Competing interests

The authors have no competing interests to declare that are relevant to the content of this article.

## 5.6 Funding

No funding was received for conducting this study.

### *5.6.1 Authors' contributions*

C Sitaula conceived an idea and simulated. C Sitaula and TB Shahi revised the manuscript and proofread.

## 5.7 Acknowledgements

The authors would like to thank those researchers, who created dataset related to Monkeypox detection.

## 5.8 Authors' information

C. Sitaula  
Department of Electrical and Computer Systems Engineering,  
Monash University  
Wellington Rd, VIC 3800

TB. Shahi  
School of Engineering and Technology  
Central Queensland University

Norman Garden, QLD, 4701, Australia  
and  
Central Department of Computer Science and IT  
Tribhuvan University  
TU Rd, Kirtipur 44618, Kathmandu, Nepal

## References

1. Ahsan MM, Uddin MR, Farjana M, Sakib AN, Momin KA, Luna SA (2022) Image data collection and implementation of deep learning-based model in detecting monkeypox disease using modified vgg16. arXiv preprint arXiv:220601862
2. Ahsan MM, Uddin MR, Luna SA (2022) Monkeypox image data collection. arXiv preprint arXiv:220601774
3. Breman JG, Stenowski M, Zanotto E, Gromyko A, Arita I, et al. (1980) Human monkeypox, 1970-79. Bulletin of the World Health Organization 58(2):165
4. Chollet F (2017) Xception: Deep learning with depthwise separable convolutions. In: Proceedings of the IEEE conference on computer vision and pattern recognition, pp 1251–1258
5. Chollet F, et al. (2015) Keras. <https://github.com/fchollet/keras>
6. Deng J, Dong W, Socher R, Li LJ, Li K, Fei-Fei L (2009) Imagenet: A large-scale hierarchical image database. In: 2009 IEEE conference on computer vision and pattern recognition, Ieee, pp 248–255
7. Glock K, Napier C, Gary T, Gupta V, Gigante J, Schaffner W, Wang Q (2021) Measles rash identification using transfer learning and deep convolutional neural networks. In: 2021 IEEE International Conference on Big Data (Big Data), IEEE, pp 3905–3910
8. He K, Zhang X, Ren S, Sun J (2016) Deep residual learning for image recognition. In: Proceedings of the IEEE conference on computer vision and pattern recognition, pp 770–778
9. Howard AG, Zhu M, Chen B, Kalenichenko D, Wang W, Weyand T, Andreetto M, Adam H (2017) Mobilenets: Efficient convolutional neural networks for mobile vision applications. arXiv preprint arXiv:170404861
10. Huang G, Liu Z, Van Der Maaten L, Weinberger KQ (2017) Densely connected convolutional networks. In: Proceedings of the IEEE conference on computer vision and pattern recognition, pp 4700–4708
11. Lara JVM, Velásquez RMA (2022) Low-cost image analysis with convolutional neural network for herpes zoster. Biomedical Signal Processing and Control 71:103250
12. Nolen LD, Osadebe L, Katomba J, Likofata J, Mukadi D, Monroe B, Doty J, Hughes CM, Kabamba J, Malekani J, et al. (2016) Extended human-to-human transmission during a monkeypox outbreak in the democratic republic of the congo. Emerging infectious diseases 22(6):1014

13. Pan SJ, Yang Q (2009) A survey on transfer learning. *IEEE Transactions on knowledge and data engineering* 22(10):1345–1359
14. Reynolds MG, Emerson GL, Pukuta E, Karhemere S, Muyembe JJ, Bikindou A, McCollum AM, Moses C, Wilkins K, Zhao H, et al. (2013) Detection of human monkeypox in the republic of the congo following intensive community education. *The American Journal of Tropical Medicine and Hygiene* 88(5):982
15. Ribeiro MT, Singh S, Guestrin C (2016) "why should I trust you?": Explaining the predictions of any classifier. In: *Proceedings of the 22nd ACM SIGKDD International Conference on Knowledge Discovery and Data Mining*, San Francisco, CA, USA, August 13-17, 2016, pp 1135–1144
16. Rossum G (1995) Python reference manual. Tech. rep., Amsterdam, The Netherlands
17. Sandeep R, Vishal K, Shamanth M, Chethan K (2022) Diagnosis of visible diseases using cnns. In: *Proceedings of International Conference on Communication and Artificial Intelligence*, Springer, pp 459–468
18. Sandler M, Howard A, Zhu M, Zhmoginov A, Chen LC (2018) Mobilenetv2: Inverted residuals and linear bottlenecks. In: *Proceedings of the IEEE conference on computer vision and pattern recognition*, pp 4510–4520
19. Sarumi OA (2020) Machine learning-based big data analytics framework for ebola outbreak surveillance. In: *International Conference on Intelligent Systems Design and Applications*, Springer, pp 580–589
20. Selvaraju RR, Cogswell M, Das A, Vedantam R, Parikh D, Batra D (2017) Grad-cam: Visual explanations from deep networks via gradient-based localization. In: *Proceedings of the IEEE international conference on computer vision*, pp 618–626
21. Shahi TB, Sitaula C, Neupane A, Guo W (2022) Fruit classification using attention-based mobilenetv2 for industrial applications. *Plos one* 17(2):e0264586
22. Simonyan K, Zisserman A (2015) Very deep convolutional networks for large-scale image recognition. In: *International Conference on Learning Representations*
23. Sitaula C, Hossain MB (2021) Attention-based vgg-16 model for covid-19 chest x-ray image classification. *Applied Intelligence* 51(5):2850–2863
24. Sitaula C, Basnet A, Mainali A, Shahi TB (2021) Deep learning-based methods for sentiment analysis on nepali covid-19-related tweets. *Computational Intelligence and Neuroscience* 2021
25. Sitaula C, Shahi TB, Aryal S, Marzbanrad F (2021) Fusion of multi-scale bag of deep visual words features of chest x-ray images to detect covid-19 infection. *Scientific reports* 11(1):1–12
26. Szegedy C, Vanhoucke V, Ioffe S, Shlens J, Wojna Z (2016) Rethinking the inception architecture for computer vision. In: *Proceedings of the IEEE conference on computer vision and pattern recognition*, pp 2818–2826
27. Tan M, Le Q (2019) Efficientnet: Rethinking model scaling for convolutional neural networks. In: *International conference on machine learning*,

PMLR, pp 6105–6114

28. World health organization (2022) Multi-country monkeypox outbreak: situation update. <https://www.who.int/emergencies/diseases-outbreak-news/item/2022-DON396>, (Accessed: 2022-06-30)